Highly Ordered Nanoporous Template from Triblock Copolymer

Dong Hyun Lee,[†,§] Soojin Park,[‡] Weiyin Gu,[†] and Thomas P. Russell[†,*]

[†]Polymer Science and Engineering Department, University of Massachusetts, Amherst, Massachusetts 01003, United States, and
[‡]Interdisciplinary School of Green Energy, Ulsan National Institute of Science and Technology (UNIST), Ulsan 689-798, Korea.
[§] Present address: Advanced Light Source (ALS), Lawrence Berkeley National Lab, Berkeley, CA 94720, U.S.A.

ABSTRACT Silica nanoporous templates from poly(1,4-isoprene)-*block*-polystyrene-*block*-poly-(2-vinyl pyridine) (IS2VP) were prepared. The films of IS2VP spin-coated from toluene showed a dimple-type structure with short-range lateral order. When the films were exposed to a mixed solvent vapor of toluene/hexane, a highly ordered and oriented core−shell structure, consisting of an outer shell of PI, a middle shell of PS, and a core of P2VP, was obtained. The PI was degraded by UV-ozone treatment and removed. A film of polydimethylsiloxane (PDMS) was spin coated onto the remaining film with dimple-type structures and, upon heating, was drawn into the interstitial regions by capillary action. Exposure to oxygen plasma converted the PDMS into silica and degraded all other remaining polymers. This led to highly ordered and oriented nanoporous silica that could be used as an etching mask for transfer of the pattern or templates for metal loading.

KEYWORDS: nanoporous templates · triblock copolymer · highly ordered nanostructure · solvent-annealing · core−shell structure

Block copolymers (BCPs) consisting of chemically distinct polymers linked by a covalent bond at one end have the ability to self-assemble into a variety of ordered nanostructures. Depending upon volume fraction of the components, BCP nanoscopic microdomains, like body-centered cubic spheres (BCC), hexagonally packed cylinders (HEX), lamellae (LAM), and bicontinuous gyroids are prepared at certain conditions.[1−4] The molecular weights of the BCP and the individual blocks can be varied to control the size and separation distance of the nanoscopic domains. Porous materials have gained much attention for use in catalysis,[5] as scaffolds or templates for nanomaterial synthesis,[6] cell culture substrates,[7] separation media,[8] and antireflection coatings.[9] Porous templates for these applications have been generated by templating techniques using arrays of polymer latex particles,[10,11] condensation of water droplets,[12,13] colloidal silica,[14] or BCPs.[15−17] Among these, BCPs offer versatility in the size, uniformity, and periodicity of the pores. However, it is necessary to control the alignment of BCP microdomains to achieve two-dimensional (2D) arrays of nanopores that span the thickness of the film. A number of approaches have been used to fabricate highly ordered nanostructures from BCP thin films, including tailored interfacial interactions,[18−21] solvent annealing,[22−24] electric fields,[25,26] chemical patterning of substrates,[27,28] graphoepitaxy,[29,30] and epitaxial growth.[31,32] Among these approaches, solvent annealing has proven to be rapid, applicable to numerous BCPs, simple to implement, and does not require a special pretreatment of the substrate used. While the structures produced by solvent annealing are nonequilibrium structures, numerous methods are available to freeze in the structures produced.

In this study, we show that long-range ordering of hexagonally packed core−shell nanostructures of poly(1,4-isoprene)-*block*-polystyrene-*block*-poly(2-vinylpyridine) copolymers (IS2VP) can be achieved over the macroscopic length scale by solvent annealing in a mixed vapor of toluene/hexane. Furthermore, well-ordered nanoporous silica templates containing Au nanoparticles were fabricated by sequential UV−ozone and oxygen plasma treatments. Many research groups reported that well-ordered BCP thin films could be directly used as templates or scaffolds to generate periodic arrays of nanoparticles.[33,34] Despite advances in the production of a spatial array of nanoparticles, the way to localize an individual nanoparticle into a pore of the template has not yet been reported. In addition, although a sol−gel process also can be used for producing multimetallic nanoparticles, this procedure is very restrictive in the control of the spatial position of the nanoparticles.[35] However, the core−shell nanostructure based on triBCP that we have established here is able to not only produce periodic arrays of nanoparticles but also effectively localize them in a silica nanoporous template because the P2VP core can offer the strong interaction with metallic

*Address correspondence to russell@mail.pse.umass.edu.

Received for review October 20, 2010 and accepted January 8, 2011.

Published online February 03, 2011
10.1021/nn102832c

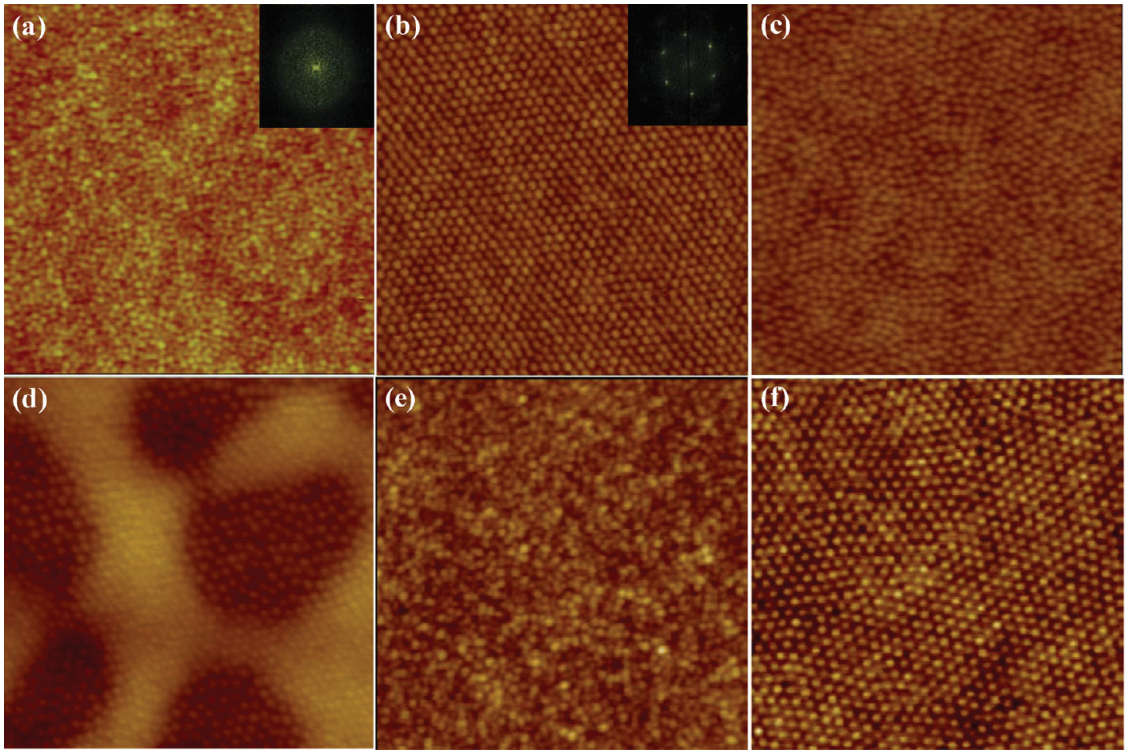

Figure 1. SFM images (1.5 μm $\times$ 1.5 μm, height mode) of (a) as-spun of IS2VP80, and IS2VP films annealed in solvent vapor for (b) 60 min, (c) 90 min, (d) 210 min, and (e) as-spun of IS2VP99, (f) IS2VP99 annealed for 60 min.

precursors, even though the PI external shell creates enough space for the silica well by degradation of itself. Here, we show that solvent annealing of IS2VP films generates well-defined core−shell nanostructures on silicon substrates, and the nanoporous templates can be produced from the solvent-annealed IS2VP films.

RESULTS AND DISCUSSION

Figure 1 shows SFM images of as-spun and solvent-annealed IS2VP thin films at various annealing times. IS2VP80 triBCP films spin-coated onto a silicon substrate from a 0.7 wt % toluene solution show a dimple-type structure having an average diameter of 33 nm with short-range lateral order (Figure 1a). The fast Fourier transform (FFT) of the data in Figure 1a shows a diffuse circular pattern which is characteristic of short-range order. When the as-spun film was annealed in the vapor of toluene/hexane (70/30, v/v) mixture for 60 min, well-defined hexagonally packed nanostructures with an average diameter of 36.8 nm were observed (Figure 1b). FFT of the SFM image shows six strong spots, which are characteristic of a hexagonally packed structure with long-range lateral ordering of the nanostructures. It is noteworthy that we can properly control the solvent-annealing conditions for inducing triBCP nanostructures because our cleaning process with oxygen plasma can enhance the wettability of triBCP films on the Si substrate by producing a silanol group on its surface. With longer solvent-annealing time (90 min), the ordering of the BCP microdomains is lost on the surface, as shown by the SFM image in Figure 1c. A dewetting of the film is also evident in the data shown in Figure 1d. Consequently, solvent annealing times were restricted to ~60 min. The thin films of IS2VP99 were also prepared in the same manner with IS2VP80. SFM image of as-spun films of IS2VP99 also showed short-range order of dimple-type structures (Figure 1e). However, after solvent-annealing in the vapor of toluene/hexane (70/30, v/v) mixture for 60 min, a long-range ordering of hexagonal arrays of nanostructures was observed on the whole surface area of the Si substrates as shown in Figure 1f. We also found that the mixed solvent containing lower content of hexane led to dewetting of thin films under the same annealing conditions.

Since SFM provides information on the local ordering of BCPs, another tool for confirmation of the ordering over macroscopic distances is necessary. This was accomplished with grazing incidence small-angle X-ray scattering (GISAXS) measurement. The GISAXS data of the as-spun IS2VP80 film in Figure 2a show just a pair of broad diffraction peaks along q_y, the scattering vector in the plane of the film, where $q = (4\pi/\lambda)\sin(\theta/2)$, θ is the scattering angle and λ is the wavelength. The X-ray profile along q_y shows a broad, first-order scattering peak (q^*) corresponding to a d-spacing of ~32 nm which is in good agreement with SFM data in Figure 1a. The GISAXS reflections are also extended along q_z, that is, normal to the surface, resulting from a truncation of the structures at the surface of the films. The GISAXS

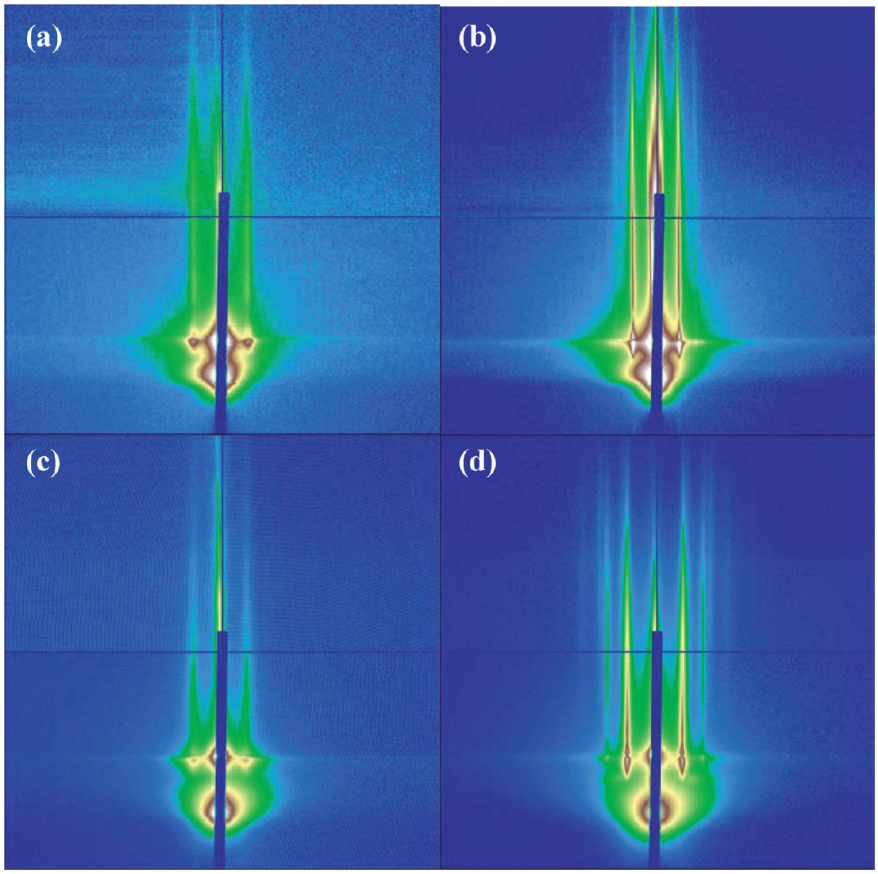

Figure 2. GISAXS 2D images (abscissa: q_y axis, ordinate: q_z axis) of (a) as-spun and (b) solvent-annealed IS2VP80 film and (c) as-spun and (d) solvent-annealed IS2VP99.

data in Figure 2b of the IS2VP80 film solvent-annealed for 60 min, followed by immersing into ethanol for surface reconstruction shows two strong diffraction peaks, corresponding to a *d*-spacing of 39 nm, and several higher order reflections which are characteristics of the long-range ordering. As evidenced by the scattering peaks at q^*, $\sqrt{3}q^*$, and $\sqrt{4}q^*$, the morphology consists of hexagonally packed cylindrical microdomains oriented normal to the film surface, as evidenced by the extension of the scattering along q_z and the lack of any out-of-plane reflections. It is interesting to note the difference of *d*-spacing between the as-spun and solvent-annealed IS2VP film. For the as-spun film, the PI and PS blocks are not perfectly segregated, since the sample was cast from toluene, a good solvent for both blocks. Consequently, the nanostructures of the as-spun film are composed of a shell of partially mixed PI and PS and a core of P2VP. In contrast, during solvent annealing in toluene/hexane vapors, hexane induces the microphase separation of the PI and PS blocks. Moreover, the solvent annealing has led to a significantly enhanced long-range ordering of hexagonal array of nanostructures. As displayed in Figure 2c, the as-spun IS2VP99 thin film showed the broad first order scattering peak along ther q_y axis, which means a short-range of the dimple structure. However, as the thin film was solvent-annealed into the vapor of toluene/hexane mixture for 60 min, various diffraction peaks were observed in Figure 2d. Since these scattering peaks were observed at q^*, $\sqrt{3}q^*$, and $\sqrt{4}q^*$, *etc.*, it is evident that the long-range ordering of hexagonally packed nanostructures was achieved. In addition, it is found that *d*-spacing of solvent-annealed IS2VP99 thin film is 42.6 nm from the position of the first order scattering peak.

Figure 3a shows an SFM image of a solvent-annealed IS2VP80 film which is immersed into $HAuCl_4$ ethanol solution for 1 min. Because pyridine groups can be associated with Au salts, they are selectively incorporated into P2VP domains that are the cores of IS2VP triBCP thin film. To incorporate Au salts into the P2VP cores, a solvent-annealed IS2VP film was immersed in 1 wt % ethanol solution of $HAuCl_4$ for 1 min. It should be noted that hexagonal arrays of IS2VP still remain after incorporation of Au salts, even though the films were immersed in ethanol. According to some references,[23,24] when BCP thin films with P2VP cores were dipped into pure ethanol without $HAuCl_4$, surface reconstruction of the films took place because ethanol is a good solvent for P2VP. However, the association with $HAuCl_4$ of P2VP not only prevents the generation of nanopores in the film but also preserves the hexagonal arrays of IS2VP

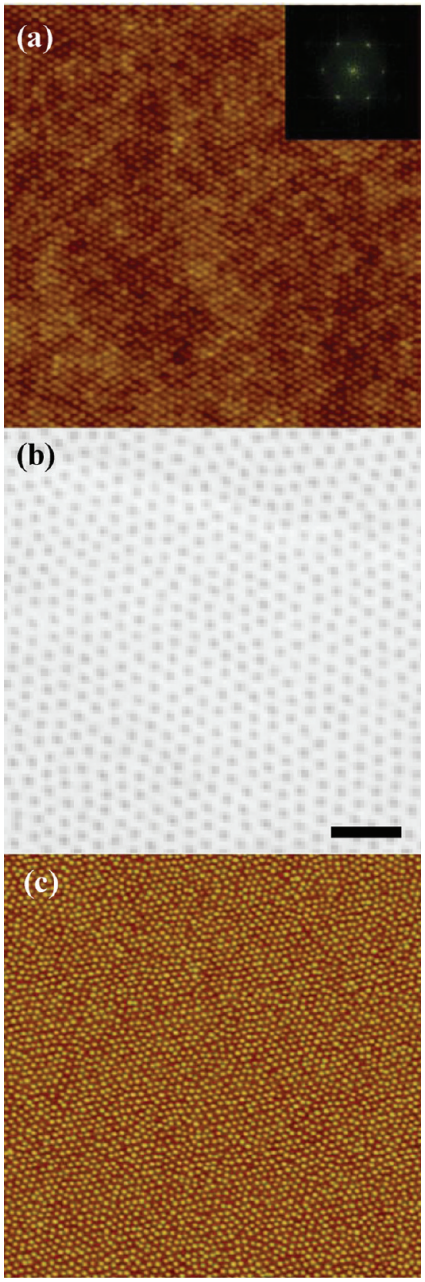

Figure 3. (a) SFM image (2.5 μm $\times$ 2.5 μm, height mode) and (b) TEM image (scale bar =200 nm) of IS2VP80 film immersed in ethanol solution of $HAuCl_4$. (c) SFM image (2.5 μm $\times$ 2.5 μm, height mode) of Au nanopartilce array from IS2VP80.

microdomains. After incorporation of gold salts to P2VP blocks, the mobility of P2VP containing gold in ethanol was significantly reduced, and thus, the nanopores were not produced. Figure 3b shows a TEM image of IS2VP film immersed into $HAuCl_4$ ethanol solution. Since the film was not stained, the dark dots can be attributed to the gold association with P2VP. Therefore, the existence of gold nanoparticles in P2VP was confirmed by TEM images in Figure 3b. To demonstrate the fabrication of nanoparticle array, the thin film of IS2VP80 containing Au salts shown in Figure 3a was

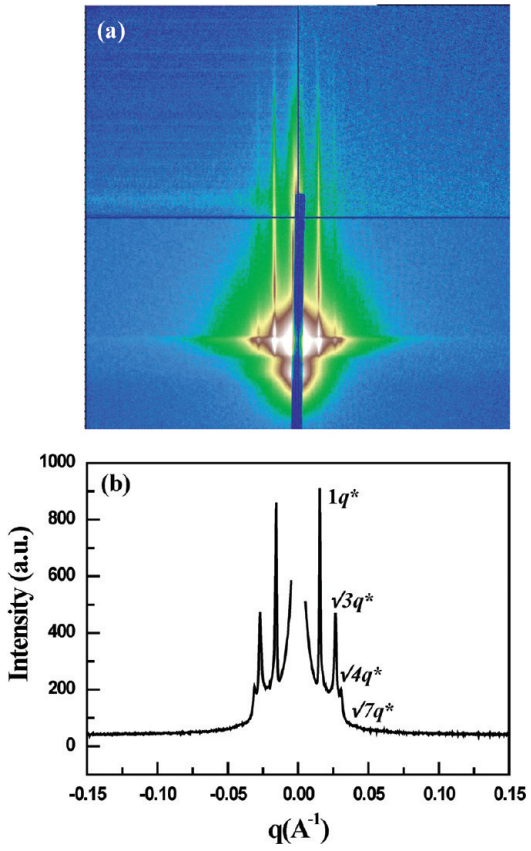

Figure 4. GISAXS profiles of gold salt containing IS2VP80 films. (a) 2D image (abscissa: q_y axis, ordinate: q_z axis) and (b) 1D profile of BCP thin films.

exposed to oxygen plasma. In result, Au salts in P2VP domains were converted to Au nanoparticles while triBCP was completely degraded as seen in Figure 3c.

To investigate long-range ordering in IS2VP films containing Au nanoparticles, GISAXS was used. As shown in Figure 4a, the GISAXS patterns show multiple strong reflections. In comparison to the GISAXS in Figure 2b, the intensity of the reflections has increased due to an increase in the electron density difference between the BCP components. The incorporation of Au into the PVP microdomains markedly changes the contrast because it can enhance the contrast of P2VP domains on X-ray reflection. But, we did not find any evidence of Au nanoparticles in this thin film. The line-scan along the q_y direction in the GISAXS pattern seen in Figure 4a shows several strong reflections of q^*, $\sqrt{3}q^*$, $\sqrt{4}q^*$, and $\sqrt{7}q^*$, indicating a hexagonal arrays of microdomains with long-range lateral ordering (Figure 4b).

Figure 5a and 5b gives the SFM images of IS2VP80 and IS2VP99 thin films after UV-ozone treatment. As seen in Figure 5a, when the IS2VP80 film containing $HAuCl_4$ was exposed shortly under UV light in the presence of oxygen, the outer shell of PI in the IS2VP film was selectively degraded and, upon rinsing with *n*-hexane to remove the degradation byproduct, 24 nm diameter core−shell nanoposts were observed over the entire surface of film with an outer shell of PS and

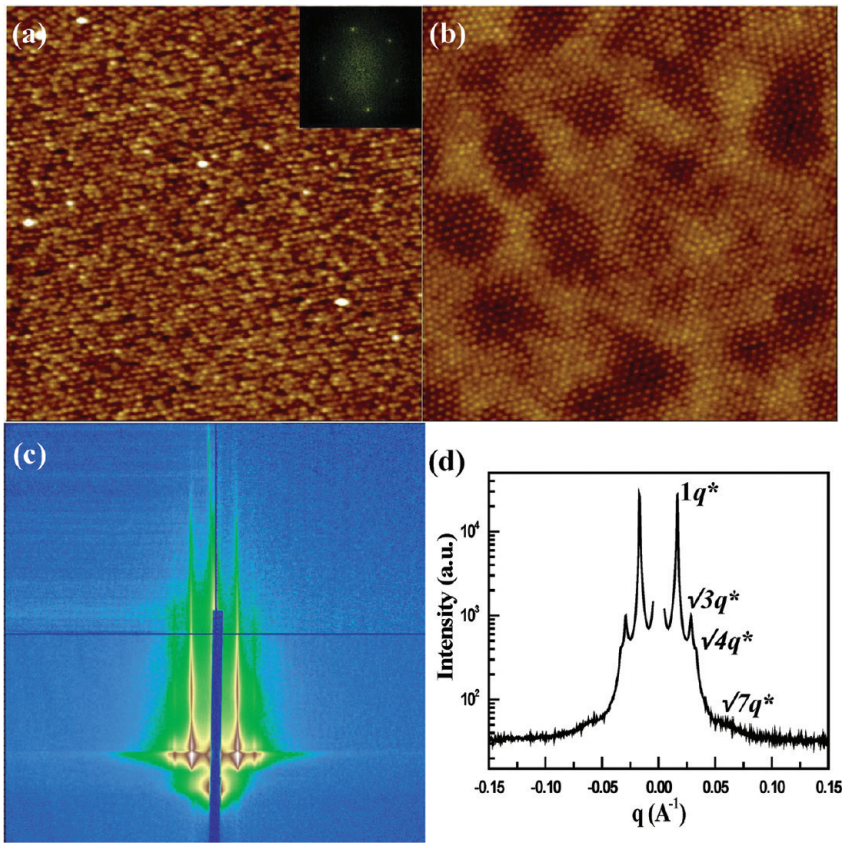

Figure 5. SFM images (2.5 μm $\times$ 2.5 μm, height mode) of (a) IS2VP80 and (b) IS2VP99 thin films after UV−ozone treatment. GISAXS profiles of IS2VP80 film after UV−ozone treatment; (c) 2D image (abscissa: q_y axis, ordinate: q_z axis) and (d) 1D profile.

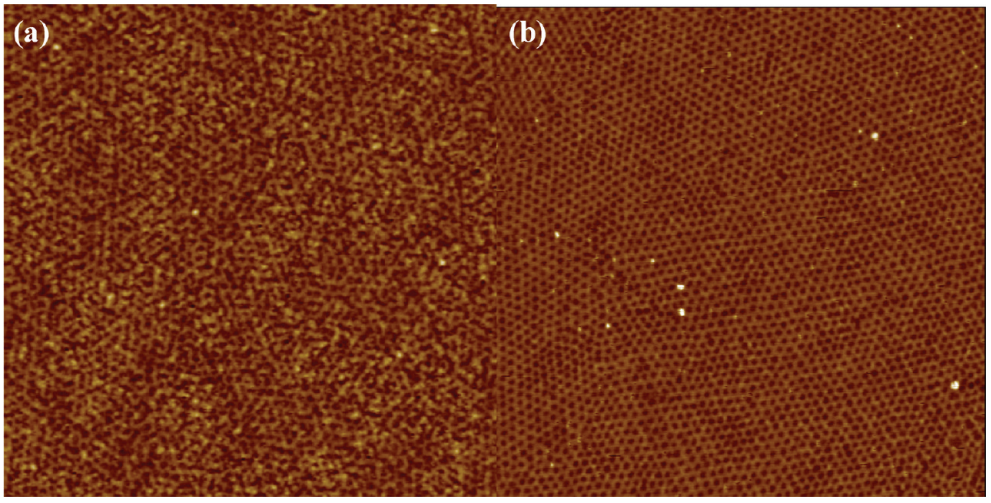

Figure 6. SFM image (3 μm $\times$ 3 μm, height mode) of silica nanoporous templates from (a) IS2VP80 and (b) IS2VP99 after oxygen plasma.

an interior of P2VP complexed with $HAuCl_4$. The corresponding FFT image of the nanopost film is shown in the inset of Figure 5a. The FFT confirms that the nanoposts were arranged on a hexagonal lattice with a high degree of lateral order. IS2VP99 thin film also shows nanoposts composed of PS and P2VP in Figure 5b as UV treatment is conducted in the same manner as in Figure 5a. Figure 5c and 5d show the GISAXS results of nanoposts obtained from IS2VP80 on a silicon wafer. Strong reflections are seen at q^*, $\sqrt{3}q^*$, $\sqrt{4}q^*$, and $\sqrt{7}q^*$ with a characteristic d-spacing of 37.7 nm. Consequently, the well-defined hexagonal arrays of the initial core−shell morphology of solvent-annealed IS2VP were maintained through sample preparation without changing the separation distance after UV-ozone treatment.

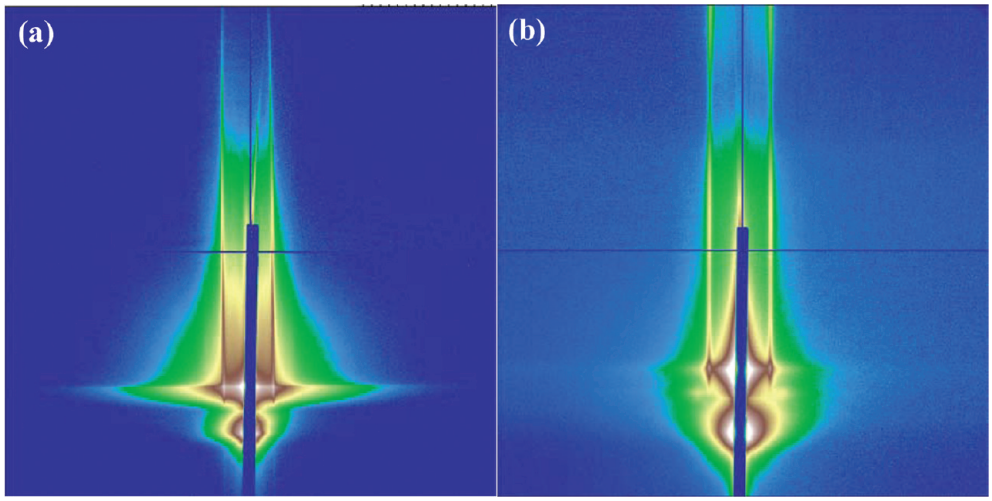

Figure 7. GISAXS profiles of silica nanoporous template after oxygen plasma treatment: (a) IS2VP80 and (b) IS2VP99.

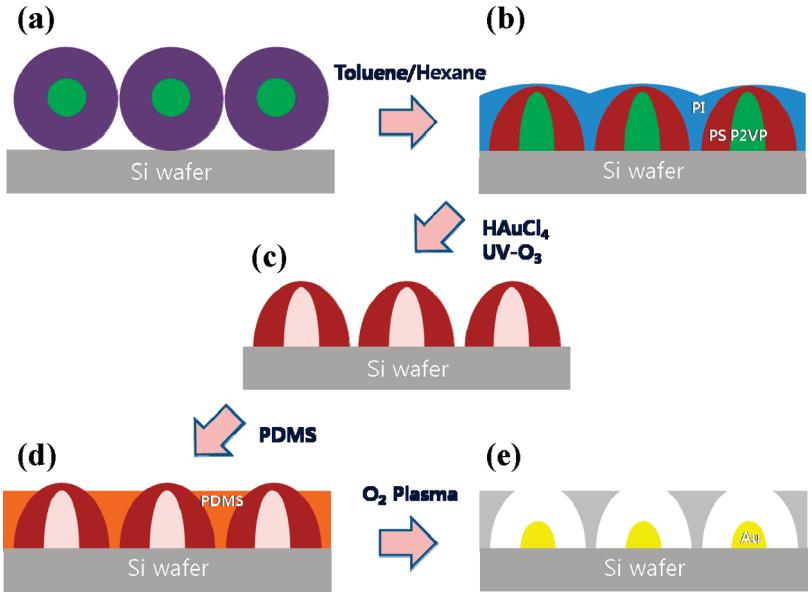

Scheme 1. Schematic illustration for preparation of silica nanoporous template. (a) As-spun IS2VP film, (b) solvent-annealed IS2VP film, (c) loading of $HAuCl_4$ into poly(2-vinylpyridine) core and removal of poly(1,4-isoprene) from IS2VP film with UV-ozone treatment, (d) spin-coating of PDMS onto the nano-pillar of PS-P2VP with Au nanoparticles, and (e) conversion of silica wall from PDMS using oxygen plasma treatment.

Figure 6 shows an SFM image of silica nanoporous template prepared from IS2VP80 and IS2VP99 thin films. To prepare the nanoporous template, PDMS was spin-coated onto nanoposts obtained by the ozonolysis of the PI block from a solvent-annealed film seen in Figure 5, then heated to 45 °C for 1 h to increase the mobility of PDMS and allow capillary force to draw the PDMS into the empty regions between the nanoposts. Using oxygen plasma, the PDMS was converted to silica and the nanoposts were completely removed. This left a silica film having a hexagonal array of nanopores with a diameter equal to that of the removed nanoposts (Scheme 1e). This observation also indicates that either pore size or separation distance of pores can be controlled by the molecular weights (or composition) of triBCP as seen in Figure 6a,b. Whereas, the PVP containing gold salts generates gold nanoparticle in each pore after oxygen plasma treatment. This simple route to place inorganic nanoparticles within each pore in a silica matrix opens the application of these nanoporous templates for surface enhanced plasmon, immobilization of DNA or organic dyes, catalysis, and epitaxial growth of the crystal.

Figure 7a shows 2D diffraction pattern of GISAXS for the nanoporous template produced from oxygen plasma treatment. Here, in contrast to previous GISAXS results, we observed a pair of strong diffraction peaks and another pair of weak reflections. The strong first order peak and weak second order peak appearing at q^*, $\sqrt{3}q^*$, as shown in Figure 7b, correspond to a hexagonal array

with a *d*-spacing of 41 nm. It should be noted that, while the hexagonal packing has been preserved, the extent of lateral ordering has been reduced during the process. Another possibility is that the thickness of sample prepared from PDMS-filled polymer films by oxygen plasma exposure was significantly decreased, and discontinuous silica layer might be formed at certain areas.

CONCLUSIONS

Using SFM and GISAXS we have shown that long-range ordering of hexagonal arrays of nanostructures of IS2VP triblock copolymer was achieved by solvent annealing in vapors of a toluene/hexane mixture. It was found that the nanostructures of IS2VP consisted of micellar arrays having an outer shell of PI, a middle shell of PS, and a core of P2VP. Immersion of IS2VP films into a 1 wt % solution of a gold salt in ethanol allowed the formation of a gold-incorporated P2VP microdomain that, subsequently, could be converted to Au nanodots. We showed that nanoporous templates containing gold nanoparticles within each nanopore could be produced by sequential UV-ozone and oxygen plasma treatments. These nanoporous templates have potential applications for surface enhanced plasmons, immobilization of DNA or organic dyes, catalysis or epitaxial growth of crystal.

EXPERIMENTAL SECTION

Materials. Two different polyisoprene-*block*-polystyrene-*block*-poly(2-vinylpyridine) (IS2VP) copolymers were purchased from Polymer Source and used without further purification in this study. The number average molecular weights (M_n) of poly(1,4-isoprene), polystyrene, and poly(2-vinylpyridine) in the IS2VP80 were 9, 60, and 11 kg/mol, respectively. The number average molecular weights (M_n) of poly(1,4-isoprene), polystyrene, and poly(2-vinylpyridine) in the IS2VP99 were 13, 70, and 16 kg/mol, respectively. And the polydispersity (M_w/M_n) of both IS2VP80 and IS2VP99 was 1.14. A schematic illustration of the process to fabricate the nanoporous templates is shown in Scheme 1. IS2VP triBCPs were dissolved in toluene to yield 0.7 and 1.0 wt % polymer solution at room temperature and stirred for 12 h. Then, IS2VP thin films were prepared by spin-coating at 3000 rpm on silicon substrates (Scheme 1a). Si ⟨100⟩ wafers (International Wafer Service Inc.) were cleaned by snow jet and oxygen plasma treatment, subsequently. The films were exposed to a mixed toluene/hexane (70/30, v/v) vapor for various times to induce microphase-separation between block components at room temperature (~23 °C) in a small closed chamber (Scheme 1b). For preparation of gold (Au) nanoparticles inside the poly(2-vinylpyridine) core, the polymer films were immersed in a 1 wt % ethanol solution of hydrogen tetrachloroaurate(III) ($HAuCl_4$) for 1 min. The films were then rinsed with ethanol several times to remove any free Au-salt and thoroughly dried in air. Subsequently, poly(1,4-isoprene) was degraded selectively by UV−ozone irradiation for 90 s (Scheme 1c). Then, films were washed with hexane which is a good solvent for polyisoprene and a nonsolvent for polystyrene and poly(2-vinylpyridine). For the fabrication of the nanoporous silica, polydimethylsiloxane (PDMS, Aldrich, M_w = 62 000 g/mol) dissolved in heptane was spin-coated onto the films, annealed at 45 °C for 1 h to enhance the mobility of PDMS and draw the PDMS into the interstitial regions (Scheme 1d). The thickness of PDMS film on thin film was controlled from 5 to 8 nm by controlling its concentration and spin-coating rate. Finally, the PDMS was transformed into silica by oxygen plasma treatment, while any remaining BCP was completely degraded (Scheme 1e).[23,36]

Characterization of Morphology in Thin Films. The surface patterns of polymer films were assessed by scanning force microscopy (SFM) in both the height and phase contrast modes using a Digital Instruments Dimension 3000 scanning force microscope operated in the tapping mode. Film thickness was measured by ellipsometry. Transmission electron microscopy (TEM) measurements were performed on a JEOL 100CX electron microsocope operated at 100 kV. For TEM measurements, the samples were prepared on silicon substrates with a thick silicon oxide (~ 250 nm) layer. Polymer films were floated onto the surface of a 5 wt % aqueous solution of HF and transferred to a Cu grid for TEM measurements. Grazing incidence small-angle X-ray scattering (GISAXS) measurements were performed at the 7.3.3. beamline at the Advanced Light Source (Lawrence Berkeley National Laboratory). Sample-to-detector (S/D) distance for IS2VP80 and IS2VP99 were 3100 and 4100 mm, respectively.

Acknowledgment. This work was supported by the US Department of Energy, Office of Basic Energy Science (TPR), NSF-supported Materials Research Science and Engineering Center (DMR-0213695) (DHL) and Center for Hierarchical Manufacturing (DMI-0531171) (SP) at the University of Massachusetts, Amherst. S.P. was also supported by the WCU (R31-2008-000-20012-0) programs. D.H.L. was supported by the Korea Research Foundation Grant funded by the Korean Government (KRF-2008-D00068) and by an LBNL Laboratory Directed Research and Development grant.

REFERENCES AND NOTES

1. Leibler, L. Theory of Microphase Separation in Block Copolymers. *Macromolecules* **1980,** *13*, 1602–1617.
2. Hashimoto, T. *Thermoplastic Elastomers*; Legge, N. R., Holden, G., Schroeder, H. E., Eds.; Hanser: New York, 1987.
3. Bates, F. S.; Fredrickson, G. H. Block Copolymer Thermodynamics: Theory and Experiment. *Annu. Rev. Phys. Chem.* **1990,** *41*, 525–557.
4. Hamley, I. W. *The Physics of Block Copolymers*; Oxford University Press: New York, 1998.
5. Skarbalak, S. E.; Suslick, K. S. Porous MoS_2 Synthesized by Ultrasonic Spray Pyrolysis. *J. Am. Chem. Soc.* **2005,** *127*, 9990–9991.
6. Melde, B. J.; Burkett, S. L.; Xu, T.; Goldbach, J. T.; Russell, T. P.; Hawker, C. J. Silica Nanostructures Templated by Oriented Block Copolymer Thin Films Using Pore-Filling and Selective-Mineralization Routes. *Chem. Mater.* **2005,** *17*, 4743–4749.
7. Li., Y.; Neoh, K. G.; Cen, L.; Kang, T. Porous and Electrically Conductive Polypyrrole−Poly(vinyl alcohol) Composite and Its Applications as a Biomaterial. *Langmuir* **2005,** *21*, 10702–10709.
8. Zalusky, A. S.; Olayo-Valles, R.; Wolf, J. H.; Hillmeyer, M. A. Ordered Nanoporous Polymers from Polystyrene−Polylactide Block Copolymers. *J. Am. Chem. Soc.* **2002,** *124*, 12761–12773.
9. Hiller, J. A.; Mendelsohn, J. D.; Rubner, M. F. Reversibly Erasable Nanoporous Antireflection Coatings from Polyelectrolyte Multilayers. *Nat. Mater.* **2002,** *1*, 59–63.
10. Gates, B.; Yin, Y. D.; Xia, Y. N. Fabrication and Characterization of Porous Membranes with Highly Ordered Three-Dimensional Periodic Structures. *Chem. Mater.* **1999,** *11*, 2827–2836.
11. Tierno, P.; Thonke, K.; Goedel, W. A. Using Paramagnetic Particles as Repulsive Templates for the Preparation of Membranes of Controlled Porosity. *Langmuir* **2005,** *21*, 9476–9481.

12. Srinivasarao, M.; Collings, D.; Philips, A.; Patel, S. Three-Dimensionally Ordered Array of Air Bubbles in a Polymer Film. *Science* **2001,** *292*, 79–83.
13. Cui, L.; Li, X.; Ding, Y.; Li, B.; Han, Y. Polymer Surfaces with Reversibly Switchable Ordered Morphology. *Langmuir* **2005,** *21*, 11696–11703.
14. Johnson, S. A.; Olliver, P. J.; Mallouk, T. E. Ordered Mesoporous Polymers of Tunable Pore Size from Colloidal Silica Templates. *Science* **1999,** *283*, 963–965.
15. Zhao, D. Y.; Feng, J. L.; Huo, Q. S.; Melosh, N.; Fredrickson, G. H.; Chmelka, B. F.; Stucky, G. D. Triblock Copolymer Syntheses of Mesoporous Silica with Periodic 50 to 300 Angstrom Pores. *Science* **1998,** *279*, 548–552.
16. Magbitang, T.; Lee, V. Y.; Miller, R. D.; Toney, M. F.; Lin, Z.; Briber, R. M.; Kim, H.-C.; Hedrick, J. L. Templating Organosilicate Vitrification Using Unimolecular Self-Organizing Polymers: Evolution of Morphology and Nanoporosity Development with Network Formation. *Adv. Mater.* **2005,** *17*, 1031–1035.
17. Chao, C.; Wang, T.; Ho, R.; Georgopanos, P.; Avgeropoulos, A.; Thomas, E. L. Robust Block Copolymer Mask for Nanopatterning Polymer Films. *ACS Nano* **2010,** *4*, 2088–2094.
18. Mansky, P.; Liu, Y.; Huang, E.; Russell, T. P.; Hawker, C. J. Controlling Polymer-Surface Interactions with Random Copolymer Brushes. *Science* **1997,** *275*, 1458–1460.
19. Hawker, C. J.; Russell, T. P. Block Copolymer Lithography: Merging "Bottom-Up" with "Top-Down" Processes. *MRS Bull.* **2005,** *30*, 952–966.
20. In La, I.; Park, Y.-H.; Nealey, S.-M.; Gopalan, P. F.; Side-Chain-Grafted, P. Random Copolymer Brushes as Neutral Surfaces for Controlling the Orientation of Block Copolymer Microdomains in Thin Films. *Langmuir* **2006,** *22*, 7855–7860.
21. Xu, T.; Kim, H.-C.; DeRouchey, J.; Seney, C.; Levesque, C.; Martin, P.; Stafford, C. M.; Russell, T. P. The Influence of Molecular Weight on Nanoporous Polymer Films. *Polymer* **2001,** *42*, 9091–9095.
22. Park, S.; Wang, J.; Kim, B.; Chen, W.; Russell, T. P. Solvent-Induced Transition from Micelles in Solution to Cylindrical Microdomains in Diblock Copolymer Thin Films. *Macromolecules* **2007,** *40*, 9059–9063.
23. Park, S.; Kim, B.; Wang, J.; Russell, T. P. Fabrication of Highly Ordered Silicon Oxide Dots and Stripes from Block Copolymer Thin Films. *Adv. Mater.* **2008,** *20*, 681–685.
24. Kim, B.; Park, S.; McCarthy, T. J.; Russell, T. P. Fabrication of Ordered Anodic Aluminum Oxide Using a Solvent-Induced Array of Block-Copolymer Micelles. *Small* **2007,** *3*, 1869–1872.
25. Morkved, T. L.; Lu, M.; Urbas, A. M.; Ehrichs, E. E.; Jaeger, H. M.; Mansky, P.; Russell, T. P. Local Control of Microdomain Orientation in Diblock Copolymer Thin Films with Electric Fields. *Science* **1996,** *16*, 931–933.
26. Thurn-Albrecht, T.; DeRouchey, J.; Russell, T. P. Overcoming Interfacial Interactions with Electric Fields. *Macromolecules* **2000,** *33*, 3250–3253.
27. Kim, S. O.; Solak, H. H.; Stoykovich, M. P.; Ferrier, N. J.; de Pablo, J. J.; Nealey, P. F. Epitaxial Self-Assembly of Block Copolymers on Lithographically Defined Nanopatterned Substrates. *Nature* **2003,** *424*, 411–414.
28. Stoykovich, M. P.; Müller, M.; Kim, S. O.; Solak, H. H.; Edwards, E. W.; de Pablo, J. J.; Nealey, P. F. Directed Assembly of Block Copolymer Blends into Nonregular Device-Oriented Structures. *Science* **2005,** *308*, 1442–1446.
29. Segalman, R. A.; Yokoyama, H.; Kramer, E. J. Graphoepitaxy of Spherical Domain Block Copolymer Films. *Adv. Mater.* **2001,** *13*, 1152–1155.
30. Segalman, R. A.; Hexemer, A.; Kramer, E. J. Edge Effects on the Order and Freezing of a 2D Array of Block Copolymer Spheres. *Phys. Rev. Lett.* **2003,** *91*, 1961011–1961014.
31. De Rosa, C.; Park, C.; Thomas, E. L.; Lotz, B. Microdomain Patterns from Directional Eutectic Solidification and Epitaxy. *Nature* **2000,** *405*, 433–437.
32. De Rosa, C.; Park, C.; Lotz, B.; Wittmann, J.; Fetters, L. J.; Thomas, E. L. Control of Molecular and Microdomains Orientation in a Semicrystalline Block Copolymer Thin Film by Epitaxy. *Macromolecules* **2000,** *33*, 4871–4876.
33. Spatz, J. P.; Mössmer, S.; Hartmann, C.; Mller, M. Ordered Deposition of Inorganic Clusters from Micellar Block Copolymer Films. *Langmuir* **2000,** *16*, 408–415.
34. Kim, H.-C.; Jia, X.; Stafford, C. M.; Kim, D. H.; McCarthy, T. J.; Tuominen, M.; Hawker, C. J.; Russell, T.P. A Route to Nanoscopic SiO_2 Posts *via* Block Copolymer Templates. *Adv. Mater.* **2001,** *13*, 795–797.
35. Grosso, D.; Boissière, C.; Smarsly, B.; Brezesinski, T.; Pinna, N.; Albouy, P. A.; Amenitsch, H.; Antonietti, M.; Sanchez, C. Periodically Ordered Nanoscale Islands and Mesoporous Films Composed of Nanocrystalline Multimetallic Oxides. *Nat. Mater.* **2004,** *3*, 787–792.
36. Brinkmann, M.; Chan, V.Z.-H.; Thomas, E. L.; Lee, V. Y.; Miller, R. D.; Hadjichristidis, N.; Avgeropoulos, A. Room-Temperature Synthesis of a-SiO_2 Thin Films by UV-Assisted Ozonolysis of a Polymer Precursor. *Chem. Mater.* **2001,** *13*, 967–972.